Superconductivity in the Parent Infinite-Layer Nickelate $NdNiO_2$

C. T. Parzyck,[1] Y. Wu,[1] L. Bhatt,[2] M. Kang,[1,3,4] Z. Arthur,[5] T. M. Pedersen,[5] R. Sutarto,[5] S. Fan,[6] J. Pelliciari,[6] V. Bisogni,[6] G. Herranz,[7] A. B. Georgescu,[8] D. G. Hawthorn,[9] L. F. Kourkoutis,[2,4] D. A. Muller,[2,4] D. G. Schlom,[3,4,10] and K. M. Shen[1,4,7,*]

[1]*Laboratory of Atomic and Solid State Physics, Department of Physics, Cornell University, Ithaca, New York 14853, USA*
[2]*School of Applied and Engineering Physics, Cornell University, Ithaca, New York 14853, USA*
[3]*Department of Materials Science and Engineering, Cornell University, Ithaca, New York 14853, USA*
[4]*Kavli Institute at Cornell for Nanoscale Science, Cornell University, Ithaca, New York 14853, USA*
[5]*Canadian Light Source, Inc., 44 Innovation Boulevard, Saskatoon, Saskatchewan S7N 2V3, Canada*
[6]*National Synchrotron Light Source II, Brookhaven National Laboratory, Upton, New York 11973, USA*
[7]*Institut de Ciència de Materials de Barcelona (ICMAB-CSIC), Campus UAB Bellaterra 08193, Spain*
[8]*Department of Chemistry, Indiana University, Bloomington, Indiana 47405, USA*
[9]*Department of Physics and Astronomy, University of Waterloo, Waterloo, Ontario N2L 3G1, Canada*
[10]*Leibniz-Institut für Kristallzüchtung, Max-Born-Straße 2, 12489 Berlin, Germany*

(Received 16 September 2024; revised 19 February 2025; accepted 7 April 2025; published 12 May 2025)

We report evidence for superconductivity with onset temperatures up to 11 K in thin films of the infinite-layer nickelate parent compound $NdNiO_2$. A combination of oxide molecular beam epitaxy and atomic hydrogen reduction yields samples with high crystallinity and low residual resistivities, a substantial fraction of which exhibit superconducting transitions. We survey a large series of samples with a variety of techniques, including electrical transport, scanning transmission electron microscopy, x-ray absorption spectroscopy, and resonant inelastic x-ray scattering, to investigate the possible origins of superconductivity. We propose that superconductivity could be intrinsic to the undoped infinite-layer nickelates but suppressed by disorder due to a possibly sign-changing order parameter, a finding which would necessitate a reconsideration of the nickelate phase diagram. Another possible hypothesis is that the parent materials can be hole doped from randomly dispersed apical oxygen atoms, which would suggest an alternative pathway for achieving superconductivity.

DOI: 10.1103/PhysRevX.15.021048

Subject Areas: Condensed Matter Physics, Materials Science

I. INTRODUCTION

A defining characteristic of many unconventional high-temperature superconductors, including the cuprates, Fe-based, and now the infinite-layer nickelates is the dome-shaped dependence of their superconducting transition temperature (T_c) on hole or electron doping [1–6]. Sharing the motif of a d^9 transition metal in a square plaquette of oxygen ions [7–10], the infinite-layer nickelates mirror the cuprates in numerous ways, including a strange metal near optimal doping and Fermi liquid behavior in the overdoped regime [11]. On the other hand, the nickelates and cuprates also display notable differences. While the undoped cuprates are antiferromagnetic charge-transfer insulators with an approximately 2 eV gap, undoped nickelates are metallic, presumably from the self-doping of the NiO_2 planes by rare-earth $5d$ states [12–17], and possess short-ranged magnetic fluctuations [18–21] in lieu of long-range Néel order. While the cuprates are well described by a single-band model, the rare-earth $5d$ and $3d_{z^2}$ orbitals may also play a role in the low-energy electronic structure of the nickelates [22,23]. Calculations also suggest important differences in the $p-d$ hybridization and relative strength of correlations in the Ni^{1+} system [24–26].

These deviations from canonical "cupratelike" behavior motivate a detailed and systematic investigation of the nature of the parent infinite-layer nickelates. While the synthesis of (undoped) infinite-layer nickelate thin films dates back to 2009, beginning with $LaNiO_2$ [27,28], signatures of superconductivity were not observed in the undoped compounds until 2021, in CaH_2 reduced $LaNiO_2/SrTiO_3$ ($T_c < 5$ K) [29], following significant

*Contact author: kmshen@cornell.edu

improvements in the sample quality in the intervening years. The quality of reduced films is sensitive to several factors, including the quality of the perovskite precursor [30], substrate imposed strain [11], film thickness and capping [31,32], and reduction method [33], as evidenced by the significant variation in residual resistivities of literature films [1,10,27–29,32–38]. One of the particular challenges in producing high-quality undoped samples is removing sufficient oxygen to reach the low valence state Ni^{1+}, compared to hole-doped compounds $Ni^{1+\delta}$, where the relaxed target valence can ease the reduction process [39,40].

Here, we report superconductivity in the infinite-layer parent compound $NdNiO_2$ with onset T_c's up to 11 K in thin films prepared using a combination of molecular beam epitaxy and atomic hydrogen reduction. A series of 20-unit-cell (u.c.)-thick samples, capped with 2–3 u.c. of $SrTiO_3$, were synthesized under nearly identical conditions, enabling a highly systematic study employing a combination of electrical transport, high resolution scanning transmission electron microscopy (STEM), x-ray absorption spectroscopy (XAS), and resonant inelastic x-ray scattering (RIXS). Among these nominally identically prepared samples, roughly one in three exhibit partial superconducting transitions while the rest display metallic behavior—without systematic differences between the two sets in lab-based x-ray diffraction measurements [41]. We conclude that the most likely scenario is that superconductivity is intrinsic to the clean limit of the undoped parent nickelates but is readily suppressed by disorder. We also speculate on the possibility of hole doping of the NiO_2 planes from randomly dispersed apical oxygen atoms. Either of the two scenarios would have important implications: If superconductivity is intrinsic to the parent compounds, this would suggest that the current phase diagram should be revisited. If excess oxygen is responsible, this would indicate a powerful alternative route for hole doping and achieving superconductivity.

II. RESULTS

We show resistivity measurements on a series of $NdNiO_2$ samples, where a significant fraction show partial superconducting transitions [Fig. 1(a)], while others exhibit metallic behavior [Fig. 1(b)]. Residual resistivities ρ_{res} were extrapolated from the normal state resistance as $T \to 0$; in superconducting samples, the normal state resistance was obtained by suppressing the downturn with an applied magnetic field, as depicted in Fig. 1(d). Values of ρ_{res} typically lie in the $300 - 700$ μΩ−cm range, significantly lower than other undoped $NdNiO_2$ films in the literature ($\rho_{res} \approx 2500$–6000 μΩ−cm) [37,50,51].

For superconducting samples, the transition region is shown in greater detail in Fig. 1(c), where the onset is apparent between 5 and 11 K. Although none of the samples exhibit a zero-resistance state down to 1.8 K, the most complete transitions are those of films grown on $(LaAlO_3)_{0.3}(Sr_2AlTaO_6)_{0.7}$ (LSAT), which also have the highest onset T_c's. The superconducting nature of the transition is confirmed by application of a magnetic field in Fig. 1(d), which fully suppresses the transition by approximately 7 T for films on $SrTiO_3$ and approximately 9 T for films on LSAT.

We define the onset transition temperature T_c^{on} as the temperature at which the resistance decreases by 2% from its normal state value, as determined from high-field measurements; in Fig. 1(e), we plot T_c^{on} versus ρ_{res} for all samples, illustrating that ρ_{res} of nearly all superconducting samples are clustered below the quantum of resistance per NiO_2 plane ($\rho_{res} < \rho_Q = hd/e^2 \approx 850$ μΩ−cm, where $d = 3.285$ Å), similar to previous reports where a downturn was reported in doped and undoped $(La, Sr)NiO_2$ [29]. This suggests that disorder could play a key role in suppressing superconductivity in the undoped nickelates and would be consistent with evidence from terahertz [52] and penetration depth measurements [53] that the infinite-layer nickelates possess a nodal, possibly *d*-wave, superconducting order parameter, since all impurities in nodal superconductors should be pair breaking [54,55]. This is supported by the fact that samples grown on LSAT exhibit higher T_c^{on}, lower ρ_{res}, and more complete superconducting transitions, likely attributable to the improved crystalline quality and reduced propensity for defects due to the better lattice match between $NdNiO_3$ and LSAT [11,38]. It remains a possibility, however, that enhancement of the T_c in films on LSAT may also result from the compressive strain imposed on the resulting reduced films, as suggested by recent transport [56] and spectroscopy studies [57].

The broad nature of the transitions and lack of a zero resistance state both suggest that the superconductivity is inhomogeneous on the millimeter scale on which measurements were performed. Throughout this manuscript, we refer to nanometer-scale defects and imperfections in the crystalline lattice as *disorder*, including point or line defects generated during growth and reduction. On the other hand, we refer to nonuniformity in the level of the aforementioned disorder on more macroscopic (i.e., 10 μm–1 mm) length scales as *inhomogeneity*. Such macroscale inhomogeneity may include a nonuniform distribution of defects or chemical gradients (i.e., oxygen nonstoichiometry) arising during the reduction process due to a spread in the atomic hydrogen beam or thermal gradients. This raises the question: Does the observed superconductivity originate from tiny (i.e., < 1%) amounts of a filamentary secondary phase? To rule this out, we have performed pulsed *I-V* measurements [Fig. 1(f)], which show that the sample accommodates currents as high as 5–10 mA, resulting in an estimated critical current density (J_c) in the 10^4 A/cm^2 range, before fully returning to the normal state. This measurement was performed in an unconstrained geometry, with J_c estimated using a simple analytic model [58]. Though this model likely

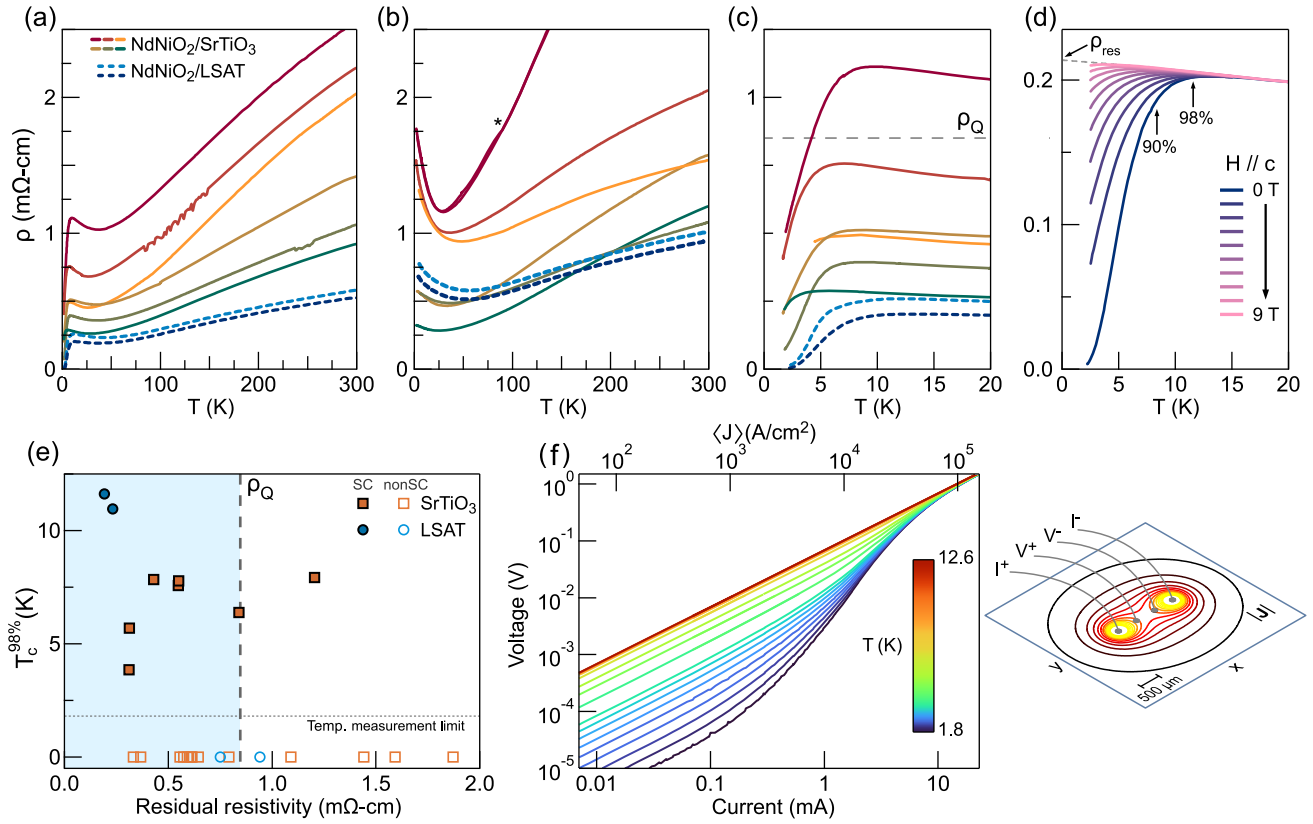

FIG. 1. Electrical transport measurements of 20-u.c.-thick $NdNiO_2$ films grown on (001) $SrTiO_3$ and (001) $(LaAlO_3)_{0.3}(Sr_2AlTaO_6)_{0.7}$ (LSAT) capped with 2–3 u.c. of $SrTiO_3$. (a) Resistivity of a series of films which display partial superconducting transitions. (b) Resistivity of a representative series of films which do not exhibit signs of superconductivity. The onset of a small hysteretic transition in a high-resistance sample at approximately 90 K is marked with a star. (c) Enlarged transition region for traces in (a). The dashed line represents the resistivity corresponding to the quantum sheet resistance per NiO_2 plane, ρ_Q. (d) Superconducting transition of an $NdNiO_2$ film on LSAT under an applied magnetic field parallel to the c axis, in 1 T steps. Arrows mark where the zero-field resistance drops to 90% and 98% of the normal state resistance. The residual resistivity ρ_{res} is extracted from the normal state resistance extrapolated to 0 K (dashed line). (e) Extracted onset T_c^{on} (defined by a 2% drop below the normal state resistance) plotted versus the film residual resistivity ρ_{res} (defined as the extrapolated normal state resistance to 0 K using high field data for superconducting samples). (f) Pulsed I-V measurements of the same film as in (d) measured between equally spaced (500 μm) leads in the pictured geometry. The estimated average current density between the voltage leads, $\langle J \rangle$, assuming a uniform and isotropic resistivity, is provided on the top axis.

overestimates J_c, the extracted value is comparable to prior measurements of optimally doped samples ($J_c \approx 1.0$–3.5×10^5 A/cm^2) [35,59] when adjusted for the reduced values of both T_c (≤ 11 K) and H_{c2} (≤ 8 T) in the undoped samples. This suggests that superconductivity likely exists throughout a substantial fraction of the sample (20%–40%), since, if only a small volume fraction of the sample were superconducting ($< 10\%$), J_c should be far lower than observed. Nevertheless, a significant number of samples with $\rho_{res} < \rho_Q$ do not superconduct, raising questions about whether disorder is the only relevant variable. Some alternative scenarios include the hole doping from residual apical oxygens left behind during the reduction process, or from Sr diffusion, resulting in $Nd_{1-x}Sr_xNiO_2$ inclusions.

We first rule out the possibility of Sr interdiffusion from either the substrate or capping layer through a combination of electrical transport and STEM measurements. Sr diffusion would be most likely during film synthesis ($T \sim 500$–550° C) rather than the reduction stage, which is brief and occurs at lower temperatures ($T \sim 300$ °C). In perovskite $NdNiO_3$, it is well established that small amounts of hole doping ($x \leq 0.06$) completely suppress the low-temperature insulating state [60–63]. In contrast, all of our unreduced $NdNiO_3$ samples, whether capped or uncapped, exhibit sharp metal-to-insulator transitions [Figs. 2(a) and 2(b)] with a nearly 10^4 increase in resistivity, excluding the possibility of Sr doping. Furthermore, annular dark field (ADF) STEM measurements on a reduced, superconducting $NdNiO_2$/LSAT film show well-defined film-substrate and film-cap interfaces [Figs. 2(c) and 2(d)] without noticeable mosaicity or planar fault formation in the $SrTiO_3$ capping layer, which occurs when the Sr nonstoichiometry exceeds 10% [64,65]. Given how thin the $SrTiO_3$ cap is (3 u.c.) relative to the $NdNiO_2$

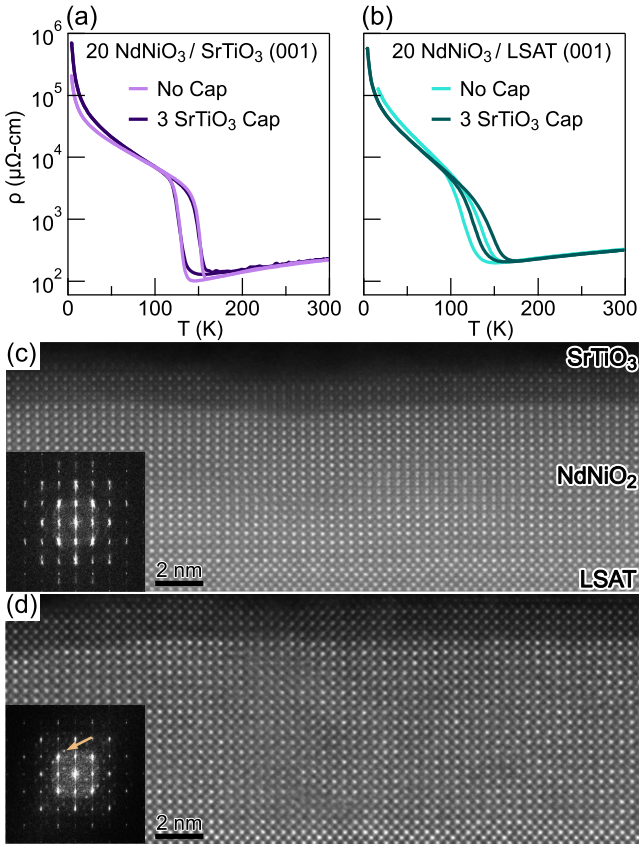

FIG. 2. Investigation of Sr interdiffusion into $NdNiO_2$. (a),(b) Electrical resistivity of 20-u.c.-thick, undoped, unreduced perovskite $NdNiO_3$ films grown on $SrTiO_3$ and LSAT, with and without $SrTiO_3$ capping layers. (c) ADF-STEM measurements of a superconducting $NdNiO_2$/LSAT film showing a region without $3a_0$ oxygen ordering. (d) Image of a different region of the same film showing $3a_0$ order. Fourier transforms of the ADF images are inset with the fractional 1/3 order peak highlighted by an arrow.

film (20 u.c.), this rules out significant Sr doping, since doping even 25% of the nickelate film into the superconducting dome ($x \sim 13\%$) would require more than 20% Sr loss from the capping layer. The presence, however, of $3a_0$ ordered regions associated with the oxygen-rich phase, $Nd_3Ni_3O_8$, in Fig. 2(d) highlight the potentiality of oxygen nonstoichiometry in our films. Though the ordered excess-oxygen phase, $Nd_3Ni_3O_8$, is itself insulating [66], the possibility of residual, unordered oxygen existing at a lower concentration motivates further investigation for signatures of inadvertent doping.

Comparing the concentration of holes in the NiO_2 plane across samples should be a direct way of distinguishing whether superconductivity is intrinsic to undoped $NdNiO_2$ or if it arises from inadvertent additional hole doping from residual apical oxygens, or other sources. Prior studies have demonstrated that XAS and RIXS spectra at the Ni L_3 edge are sensitive to hole doping [21,67]. In XAS, the undoped parent compound displays a single peak corresponding to a $2p^63d^9 \rightarrow 2p^53d^{10}$ transition, and upon hole doping, a clear shoulder emerges approximately 1 eV above the main peak (attributed to singlet holes doped into the Ni $d_{x^2-y^2}$ orbital). In Fig. 3(a), we compare representative Ni L-edge XAS spectra from superconducting and nonsuperconducting $NdNiO_2$. The spectra are nearly identical, both exhibiting a sharp, single Ni L_3 absorption peak at 852.4 eV and a strong dichroic response, consistent with previous measurements of undoped $NdNiO_2$ [67]. In Figs. 3(b) and 3(c), we show a comparison of the Ni L_3 edge from a large number of samples, with the superconducting samples exhibiting primarily a singly peaked line shape with only a weak higher-energy shoulder, whereas the nonsuperconducting samples [Fig. 3(b)] display far more variability, with stronger shoulders or even secondary peaks.

To compare the line shapes quantitatively, we fit each of the spectra with a canonical undoped $NdNiO_2$ line shape [extracted from Ref. [67] and shown in the inset in Fig. 3(d) in green] and extract the area above the undoped $NdNiO_2$ line shape (A_2, in shaded yellow). We define the normalized excess spectral weight y to be the ratio of A_2 to the total XAS intensity integrated between 852.4 and 857 eV (i.e., $A_1 + A_2$); $y = A_2/(A_1 + A_2)$. By this definition, undoped $NdNiO_2$ would have $y = 0$, while hole doping will increase y through the increasing shoulder at approximately 853.2 eV. We note that partially reduced insulating phases such as $Nd_3Ni_3O_8$ also exhibit peaks in the same energy range [66,68], so this definition of y does not distinguish between hole doping versus the presence of other impurity phases. Detailed spectroscopic studies of the lightly doped nickelates are still forthcoming, so uncertainty remains about the precise line shape in this regime and at what doping it is readily distinguishable from undoped $NdNiO_2$. Most generally, we can bound the doping from above by $x = 12.5\%$, at the boundary of the superconducting dome for $(Nd, Sr)NiO_2/SrTiO_3$. If x and y were proportionally related, then extrapolation from the 12.5% data would assign dopings of $x \leq 3\%$ to those superconducting samples with the lowest values of y on $SrTiO_3$ and LSAT.

In Fig. 3(d), we plot T_c^{on} versus y. It is notable that the majority of superconducting samples lie close to $y = 0$, resembling undoped $NdNiO_2$ and suggesting that they have minimal hole doping or impurity phases, whereas the nonsuperconducting samples exhibit a much wider degree of variability. To address whether the excess spectral weight y corresponds to doped holes or impurity phases, we note that prior studies show that ρ_{res} decreases markedly with increasing hole doping [11,50,69], so if y corresponds to doped mobile holes, then ρ_{res} should decrease monotonically with increasing y, as it does for underdoped $Nd_{1-x}Sr_xNiO_2$ (shown in dashed gray). In contrast, we find, in Fig. 3(e), that samples with the lowest ρ_{res} also have the lowest values of y, indicating that increasing y does not correspond to the doping of mobile holes into the NiO_2

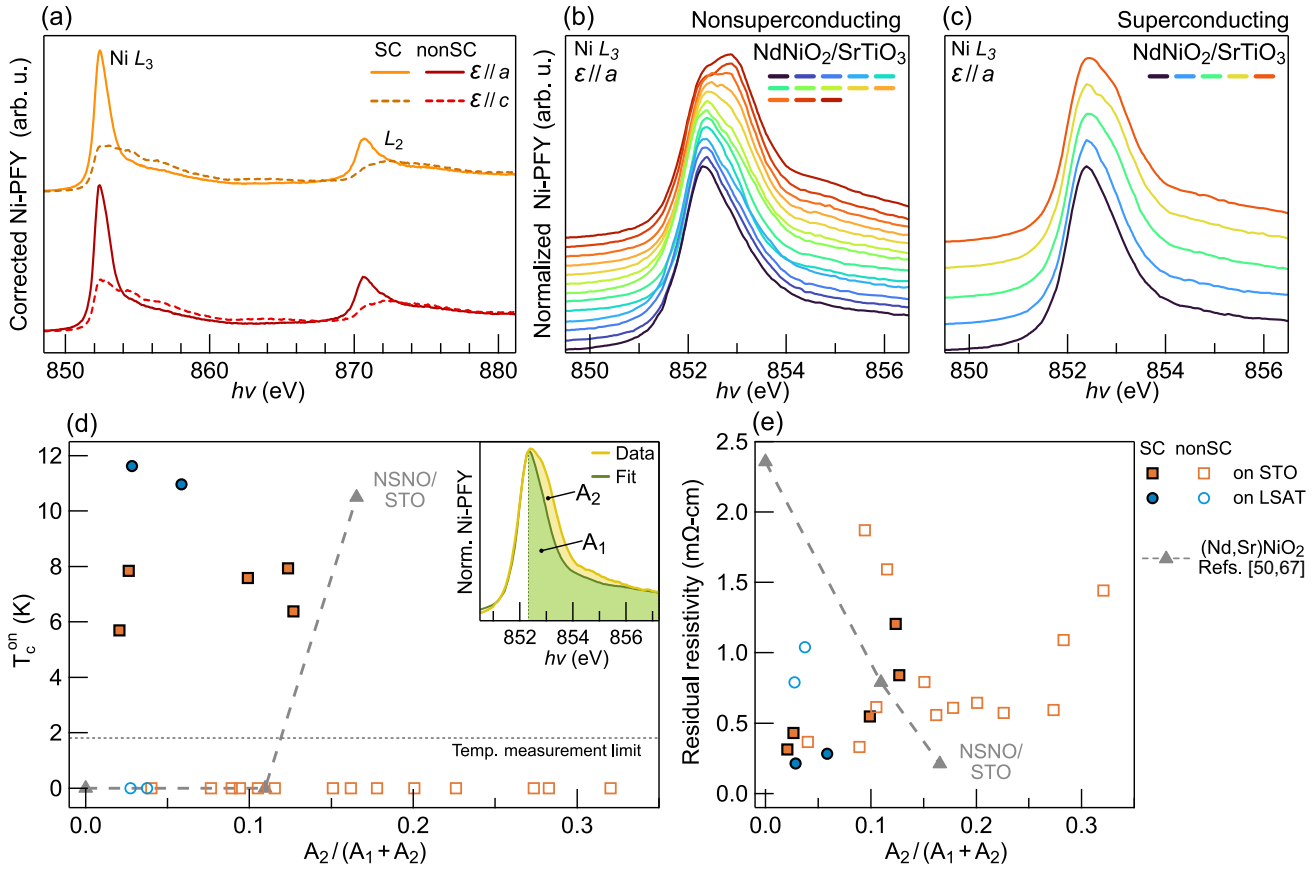

FIG. 3. XAS measurements of $NdNiO_2$. (a) Self-absorption corrected Ni L-edge partial fluorescence yield (PFY) measurements of superconducting and nonsuperconducting films on $SrTiO_3$, collected at an incidence angle of $\theta = 20°$ in σ and π polarization such that $\varepsilon \| a$ in σ polarization. $\varepsilon \| c$ signal is determined by decomposing the π-polarized data, $I = [I_\pi - I_\sigma \sin^2(20°)]/\cos^2(20°)$. (b) Ni L_3 PFY measurements of $NdNiO_2/SrTiO_3$ films not exhibiting superconducting transitions. (c) The same, for films exhibiting signatures of superconductivity. Traces in (b) and (c) have been normalized to their maximum value and offset for clarity. (d) T_c^{on} versus excess spectral weight above the undoped $NdNiO_2$ line shape, as defined in the inset, for samples on $SrTiO_3$ (squares) and LSAT (circles) substrates. (e) Comparison of ρ_{res} versus excess spectral weight. In (d) and (e), literature data for three underdoped $Nd_{1-x}Sr_xNiO_2$ samples extracted from Refs. [50,67] are provided for reference (triangles); dashed lines are a guide to the eye.

plane but more likely the presence of inclusions of insulating, partially reduced phases such as $Nd_3Ni_3O_8$. This conclusion is supported by a careful analysis of the STEM images which show that, while the majority of the sample is in the infinite-layer phase, there still exist small clusters where excess apical oxygens remain and form oxygen ordered structures, as evidenced by 1/3 order peaks in the Fourier transform of the ADF images, shown in Fig. 2(d) and Supplemental Material [41]. Prior work has identified these intermediate, oxygen ordered structures to be electrically insulating [66] and should not be the origin of the superconductivity. Taken as a whole, the XAS and STEM data clearly indicate the presence of excess oxygen atoms in the samples but suggest they form insulating, ordered structures rather than doping mobile holes.

In addition, prior RIXS measurements on underdoped $Nd_{1-x}Sr_xNiO_2$ have shown that the *dd* excitations and magnons soften considerably with hole doping [18,21,67]. In Figs. 4(a) and 4(c), we compare RIXS spectra from superconducting and nonsuperconducting $NdNiO_2/LSAT$ samples measured in the scattering geometry outlined in Fig. 4(b). The measured energies of the *dd* excitations (1.36 eV, d_{xy} and 1.82 eV, $d_{xz/yz}$), as well as the magnon energy (approximately 160 meV) and its dispersion from $H = 0.41$ to 0.17 not only match well with prior reports on undoped $NdNiO_2$, but are also clearly distinct from underdoped $Nd_{0.875}Sr_{0.125}NiO_2$ (shown in dashed gray, from Ref. [67]). Moreover, the spectra from the two samples are identical to within experimental uncertainty, indicating no observable difference in hole doping. In summary, a comparison of XAS and RIXS measurements on superconducting and nonsuperconducting $NdNiO_2$ shows no evidence for hole doping, with superconducting samples exhibiting absorption and inelastic excitations consistent with undoped $NdNiO_2$.

In Fig. 5, we present measurements of the Hall coefficient R_H, since $Nd_{1-x}Sr_xNiO_2$ and the other infinite-layer nickelates exhibit a marked dependence of R_H on hole

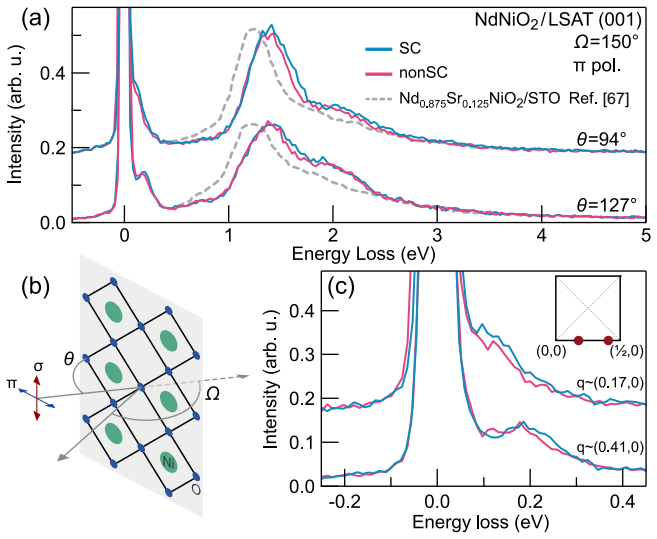

FIG. 4. Resonant inelastic scattering measurements of $NdNiO_2$ collected in π polarization at 40 K and at an incident energy 100 meV below the Ni L_3 peak (approximately 852.3 eV). (a) Comparison of energy loss spectra for superconducting and nonsuperconducting samples measured at a fixed scattering angle of $\Omega = 150°$ and incidence angles of $\theta = 94°$, 127°. Data for underdoped $Nd_{0.875}Sr_{0.125}NiO_2$ from Ref. [67] are provided for reference (dashed line). (b) Experimental geometry of x-ray absorption and inelastic scattering measurements. (c) Enlarged region around the elastic peak showing dispersive spin excitations.

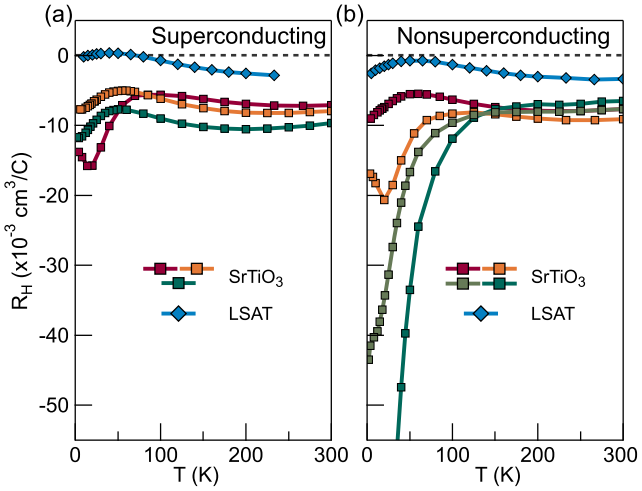

FIG. 5. Temperature dependence of the Hall coefficient, R_H, for selected 20-u.c.-thick $NdNiO_2$ films synthesized on (001) $SrTiO_3$ (squares) and (001) LSAT (diamonds) substrates. (a) Hall coefficient measurements for films exhibiting partial superconducting transitions. (b) The same, for films which do not exhibit any signs of superconductivity.

doping [29,32,36,50,69,70]. In underdoped, nonsuperconducting samples, R_H remains negative at all temperatures, but, upon traversing the superconducting dome, R_H changes sign from negative to positive below 100 K. Temperature-dependent Hall measurements are shown in Figs. 5(a) and 5(b), which indicate that, for nearly all samples, R_H remains strictly negative at all temperatures, with the exception of superconducting samples grown on LSAT. The magnitude of R_H as $T \to 0$ for samples grown on LSAT are also smaller ($-4.7 < R_H < 0.4 \times 10^{-3}$ cm^3/C) than those grown on $SrTiO_3$, consistent with prior measurements [11]. While the values of R_H (300 K) are generally consistent, the low-temperature values of R_H vary widely, similar to reports in the literature (e.g., from -40 to -6.5×10^{-3} cm^3/C [32,50,69]). These large sample-to-sample variations make drawing clear conclusions from the Hall coefficient difficult, but we note that $|R_H|$ is generally smaller for superconducting samples than for nonsuperconducting ones. Furthermore, R_H appears to be uncorrelated with ρ_{res}, suggesting that the low resistivities observed in these films are due to reduced disorder rather than hole doping consistent with the XAS measurements in Fig. 3(e).

If superconductivity arises from hole doping from residual apical oxygens, then further reduction of a superconducting sample should suppress superconductivity. In Fig. 6, we show the resistivity of a superconducting $NdNiO_2/SrTiO_3$ sample, following a sequence of short additional reduction steps. The originally reduced sample (reduction time $T_0 = 14$ min) shows a small downturn in the resistivity around 5 K. Subsequent reductions up to $T_0 + 3.5$ min *increase* T_c^{on}, but, as the sample is further reduced, superconductivity is eventually suppressed at $T > T_0 + 7.5$ min. During this sequence, no change in the x-ray diffraction pattern is observed. The erasure of the superconducting downturn and slight increase in ρ_{res} may be prescribed to some decomposition of the film from overreduction; however, the film still maintains $\rho_{res} < \rho_Q$ as T_c is suppressed, which would be more in line with the further reduction depleting the hole doping of excess oxygens. Without a method to disentangle the effects of disorder and doping from reduction, it is difficult to draw clear conclusions from this measurement. Nevertheless, the observed sensitivity of samples to the reduction process may explain why nominally identically reduced samples with $\rho_{res} < \rho_Q$ do not all show signs of superconductivity—the optimal reduction conditions for different films likely vary, depending on subtle extrinsic factors like the density of defects in the $NdNiO_3$ precursor. Further refinement of the reduction procedure and exploration of the parameter space, using either atomic hydrogen or another reducing agent, may provide a route to further improve the uniformity and reproducibility of superconducting samples. Specifically, optimization of the capping layer material and thickness, as well as the reduction procedure, may provide additional avenues to enhance the superconducting T_c and volume fraction, as in the substitutionally doped infinite-layer nickelates. Finally, while this experiment shows that superconductivity can

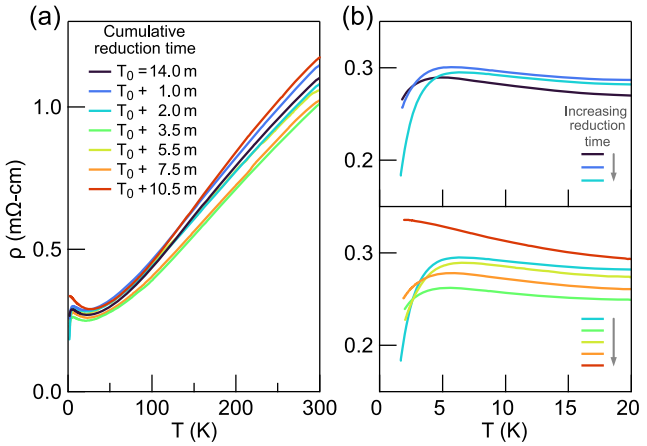

FIG. 6. Progressive reduction of an $NdNiO_2/SrTiO_3$ film. (a) Temperature-dependent resistivity of a reduced film which is subsequently exposed to additional atomic hydrogen in short intervals; reduction conditions are detailed in Supplemental Material [41]. (b) Enlarged superconducting transition region of the same data.

be suppressed by further reduction, the superconducting transitions are robust over long times (approximately 1 yr) when films are stored under ambient conditions.

III. DISCUSSION AND CONCLUSIONS

In the hole-doped cuprates, superconductivity emerges when a number of conditions are achieved: (i) holes are doped into the CuO_2 plane, (ii) the doped holes suppress long-range antiferromagnetic order, leaving short-ranged antiferromagnetic fluctuations, and (iii) the residual resistivity drops below approximately the quantum of resistance per CuO_2 plane [71,72]. It is noteworthy that the undoped parent nickelates fulfill all of the above conditions without the need for additional hole doping, lending credence to the possibility that superconductivity could be intrinsic to the parent compounds. Intrinsic superconductivity in the parent nickelate $NdNiO_2$ is also supported by our XAS and RIXS measurements, which show that the electronic structure and excitation spectra of superconducting samples closely match those from undoped $NdNiO_2$.

Furthermore, nearly all samples maintain a strictly negative Hall coefficient, consistent with the behavior of undoped infinite-layer nickelates. Together with observations of superconductivity in undoped $LaNiO_2$ [29] and, recently, $PrNiO_2$ [73], these pieces of evidence suggest that superconductivity could be intrinsic to the clean limit of the parent infinite-layer nickelates. This raises the possibility that the superconducting dome could extend all the way to $x = 0$. Such a scenario would be reminiscent of FeSe, where the undoped stoichiometric compound exhibits superconductivity without long-range antiferromagnetic order, and T_c is gradually increased with doping. To date, however, superconductivity has not been observed in lightly doped $RE_{1-x}Sr_xNiO_2$, $x = 0.05$–0.12, so it also remains a possibility that the $x = 0$ case is isolated from the neighboring dome. This motivates further study and optimization of lightly doped nickelates to better understand the potentially confounding effects of Sr doping: introducing disorder on the A site, influencing the residual oxygen (non)stoichiometry during reduction, and tuning the chemical potential.

XAS and STEM measurements provide strong evidence for the presence of residual apical oxygens but also indicate that they tend to self-organize into ordered vacancy structures such as $Nd_3Ni_3O_8$ which do not donate mobile holes [66]. Indeed, none of the measurements reported here are obviously consistent with the presence of mobile, doped holes in $NdNiO_2$. Instead, both T_c^{on} and ρ_{res} appear to be anticorrelated with the amount of excess oxygen, suggesting that the presence of excess oxygens is actually deleterious for superconductivity, as clusters of impurity phases should act as scattering centers. In the related T' and infinite-layer cuprates, excess apical oxygens do not donate mobile holes to the CuO_2 plane and rather act as strong scattering centers for low-energy quasiparticles [74,75], and their removal by postgrowth reduction is essential to achieve superconductivity.

Nevertheless, it remains difficult to unequivocally rule out the possibility of hole doping from randomly dispersed apical oxygen atoms. Indeed, the possibility that excess apical oxygens could donate mobile holes to the NiO_2 plane in the infinite-layer nickelates would be a novel finding. Controlling doping through oxygen nonstoichiometry has played a crucial role in the cuprate superconductors, enabling traversal of the phase diagrams of numerous materials such as $Bi_2Sr_2CaCu_2O_{8+\delta}$, $Tl_2Ba_2CuO_{6+\delta}$, and $HgBa_2CuO_{4+\delta}$, as well as facilitating the observation of quantum oscillations in ortho-ordered phases of $YBa_2Cu_3O_{7-\delta}$ [76]. The possibility to employ a similar tuning knob could likewise enable new approaches for realizing or enhancing superconductivity in the infinite-layer nickelates.

In conclusion, we report the observation of superconductivity with T_c onsets up to 11 K in undoped $NdNiO_2$ thin films with high crystallinity and low residual resistivities. Superconductivity appears to emerge when ρ_{res} falls below the quantum of resistance per NiO_2 sheet. We propose that superconductivity could be intrinsic to the clean limit of undoped $NdNiO_2$, as it already possesses key ingredients necessary for cuprate superconductivity, including holes in the NiO_2 plane (self-doped from rare-earth $5d$ orbitals) and short-ranged magnetic fluctuations. On the other hand, we cannot entirely rule out the possibility that residual apical oxygens could provide doped mobile holes to the NiO_2 plane, which would present a new pathway to superconductivity in the infinite-layer nickelates.

IV. METHODS

A. Sample synthesis and characterization

Thin films of $NdNiO_3$ were grown on (001)-oriented $SrTiO_3$ and LSAT substrates using reactive-oxide molecular beam epitaxy in a Veeco GEN10 system and reduced using an atomic hydrogen beam produced by flowing hydrogen gas through a thermal cracker. Details of the film growth and atomic hydrogen reduction are provided in Ref. [38]. Structural quality and phase purity of the thin film samples were determined by Cu $K\alpha_1$ x-ray diffraction measurements performed on a PANalytical Empyrean x-ray diffractometer.

Preliminary electrical transport measurements were performed using a custom built LHe-cooled four-point probe measurement station (with a base temperature of 4.2 K) using gold and indium press contacts placed near the sample corners in a square Van der Pauw geometry. Followup measurements were performed in a Quantum Design physical property measurement system (with a base temperature of 1.8 K) using a linear contact geometry, prepared by ultrasonic aluminum wire bonding, with a nominal contact spacing around 500 μm. Geometric factors in the resistivity were accounted for using the methods in Ref. [77]. Hall effect measurements were performed over the entirety of the 10×10 mm sample with wire-bond contacts placed near the sample corners in a square geometry. For one sample, however, the Hall measurements were performed using a 6-wire Hall bar geometry on a diced 5×10 mm piece. Additional details about the resistivity and Hall measurements are provided in Supplemental Material [41].

B. Pulsed *I*-*V* measurements

Pulsed *I*-*V* measurements were performed using a Keithley 6221 current source and 2182A voltmeter using a 500 μs pulse width and a variable duty cycle to maintain a fixed, low average power such that heating effects were not observable. Contacts were placed in a linear four-point geometry near the sample center with equally spaced contacts 500 μm apart. The current density $J(x, y) = |\mathbf{J}|$ can be estimated for leads placed at $x = \pm\delta$ for an infinite two-dimensional slab as described in Refs. [58,77]. The relevant quantity is then the average current density between voltage leads (spaced by $2\delta/3$): $\langle J\rangle = (3/2\delta)\int_{-\delta/3}^{\delta/3} |J(x,0)|dx$. Computing this integral provides an estimate of the constant relating $\langle J\rangle$ to the applied current I, which is $\langle J\rangle/I = 6.71 \times 10^6$ cm^{-2} for this measurement geometry. This model assumes that ρ (i) is uniform and isotropic on a macroscale and (ii) does not depend implicitly on $|\mathbf{J}|$. Both of these conditions are satisfied in the high and low current limits (when superconductivity is either unaffected or completely suppressed); however, in the intermediate regime the true value of $\langle J\rangle$ is likely smaller than predicted by this simple model. As superconductivity is quenched in the higher-density "on-axis" region, the current will spread further off axis to compensate, reducing $|\mathbf{J}|$ in the region near the leads. Because of the current spreading effect in this unconfined geometry, we cannot precisely determine the value of J_c from the data in Fig. 1(f) but can conservatively bound it between 5×10^3 and 1×10^5 A/cm^2 based on the onset and offset of the resistive transition. Further details of this estimate and the limitations of this model are provided in Supplemental Material [41].

C. Scanning transmission electron microscopy

STEM characterization was performed on a cross-sectional lamella prepared with the standard focused ion beam (FIB) lift-out procedure using a Thermo Fisher Helios G4 UX FIB. ADF imaging was performed on Cs-corrected Thermo Fisher Scientific (TFS) Spectra 300 X-CFEG or aberration-corrected TFS Titan Themis 300 operating at 300 kV and 30 mrad probe convergence semiangle. For high-precision structural measurements, a series of 40 rapid-frame images were acquired and subsequently realigned and averaged by a method of rigid registration optimized to prevent lattice hops [78] resulting in a high signal-to-noise ratio of the atomic lattice.

D. X-ray absorption spectroscopy

Nickel *L*-edge XAS measurements were performed at the SGM and REIXS beam lines of the Canadian Light Source on a tilt stage at room temperature under high vacuum; the nominal photon flux and energy resolution were $I_0 = 2 \times 10^{11}$ photons/s and $E/\Delta E \sim 8600$, respectively with a spot size of $< 30 \times 50$ μm. The incoming x-ray polarization was selected to be in either the σ ($\varepsilon\|$ to the sample a axis) or π (ε in the sample bc plane) configuration, and the fluorescence signal was measured using an array of four silicon drift detectors with an individual angular acceptance of approximately 8.02° and energy resolution of > 100 eV allowing for removal of the substantial oxygen fluorescence background produced by the substrates. PFY measurements from different detectors were corrected for self-absorption effects using the methods in Refs. [79,80], and spectra are normalized to match in the pre- (845 eV) and postedge (885 eV) regions. For O *K*-edge spectra and Ni *L*-edge spectra of samples on LSAT, substantial contributions from the substrate prevent accurate measurement of the x-ray fluorescence so total electron yield measurements were performed instead. The incident photon energy was calibrated to match prior measurements [66] performed on common samples.

E. Resonant inelastic x-ray scattering

RIXS measurements at the Ni L_3 edge were performed at the 2ID-SIX beam line at NSLS-II, Brookhaven National Laboratory (USA) at 40 K in a fixed π polarization,

to maximize the intensity of spin excitations, using the experimental geometry sketched in Fig. 4(b). The scattering angle Ω is defined as the angle between the incident and scattered x-rays and was fixed at 150° to maximize the momentum transfer. The grazing angle θ is defined as the angle between the incident x-ray and the sample surface. The selection of the resonant energy for the RIXS measurement is 0.1 eV below the main Ni absorption peak of the Ni L_3 edge, where the intensities of the spin excitations are the strongest. The energy resolution, determined by estimating the full width at half maximum of the elastic peak of a multilayer reference sample, is found to be approximately 40 meV at the Ni L_3 edge.

Note added. Recently, we have been made aware of another study reporting partial superconducting transitions in $NdNiO_2$ films grown on $NdGaO_3$ (110) [81].

ACKNOWLEDGMENTS

The authors thank Y. Birkholzer, J. Fontcuberta, H. Y. Hwang, and D. Preziosi for enlightening discussions and sharing unpublished results, as well as S. Palmer and S. Button for their assistance in substrate preparation. This work was primarily supported by the Air Force Office of Scientific Research through Grant No. FA9550-21-1-0168 and No. FA9550-23-1-0161 and also by the U.S. Department of Energy (DOE), Office of Basic Energy Sciences, under Contract No. DE-SC0019414 and the National Science Foundation through Grant No. DMR-2104427 and the Platform for the Accelerated Realization, Analysis, and Discovery of Interface Materials (PARADIM) under Cooperative Agreement No. DMR-2039380. Additional support for materials synthesis was provided by the Gordon and Betty Moore Foundation's EPiQS Initiative through Grant No. GBMF3850 and No. GBMF9073. G. H. acknowledges support from projects Severo Ochoa MaTrans42 (No. CEX2023-001263-S) and PID2023-152225NB-I00 of the Spanish Agencia Estatal de Investigación and by the Generalitat de Catalunya (2021 SGR 00445). A. B. G. was supported in part by Lilly Endowment, Inc., through its support for the Indiana University Pervasive Technology Institute. This research uses beam line 2-ID of the National Synchrotron Light Source II, a DOE Office of Science User Facility operated for the DOE Office of Science by Brookhaven National Laboratory under Contract No. DESC0012704. Part of the research described in this paper was performed using the REIXS and SGM beam lines at the Canadian Light Source, a national research facility of the University of Saskatchewan, which is supported by the Canada Foundation for Innovation (CFI), the Natural Sciences and Engineering Research Council (NSERC), the National Research Council (NRC), the Canadian Institutes of Health Research (CIHR), the Government of Saskatchewan, and the University of Saskatchewan. This work made use of the Cornell Center for Materials Research shared instrument facilities. The microscopy work was supported by NSF PARADIM (DMR-2039380), with additional support from Cornell University, the Weill Institute and the Kavli Institute at Cornell. L. B. and L. F. K. acknowledge support from the Packard foundation. The DFT calculations shown in this work have been performed on the Big Red 200 and Quartz supercomputer clusters at Indiana University. Substrate preparation was performed at the Cornell NanoScale Facility, a member of the National Nanotechnology Coordinated Infrastructure (NNCI), which is supported by the National Science Foundation (Grant No. NNCI-2025233).

C. T. P. and K. M. S. conceived the research and designed the experiment. Sample synthesis and characterization were performed by C. T. P. and Y. W. under the supervision of D. G. S. and K. M. S. X-ray absorption measurements were performed by C. T. P., M. K., Z. A., T. M. P., and R. S. and analyzed by C. T. P. and D. G. H. Resonant inelastic scattering measurements were performed by S. F., J. P., and V. B. Electron microscopy measurements were performed by L. B. under the supervision of L. F. K. and D. A. M. The results were analyzed and interpreted by C. T. P., L. B., Y. W., M. K., D. G. H., G. H., D. A. M., D. G. S., and K. M. S. Density functional theory calculations were performed by A. B. G. C. T. P. and K. M. S. wrote the manuscript with input from all authors.

DATA AVAILABILITY

The data that support the findings of this article are openly available [82].

[1] D. Li, K. Lee, B. Y. Wang, M. Osada, S. Crossley, H. R. Lee, Y. Cui, Y. Hikita, and H. Y. Hwang, *Superconductivity in an infinite-layer nickelate*, Nature (London) **572**, 624 (2019).
[2] B. Y. Wang, K. Lee, and B. H. Goodge, *Experimental progress in superconducting nickelates*, Annu. Rev. Condens. Matter Phys. **15**, 305 (2024).
[3] A. Damascelli, Z. Hussain, and Z.-X. Shen, *Angle-resolved photoemission studies of the cuprate superconductors*, Rev. Mod. Phys. **75**, 473 (2003).
[4] J. Orenstein and A. J. Millis, *Advances in the physics of high-temperature superconductivity*, Science **288**, 468 (2000).
[5] D. C. Johnston, *The puzzle of high temperature superconductivity in layered iron pnictides and chalcogenides*, Adv. Phys. **59**, 803 (2010).
[6] P. J. Hirschfeld, M. M. Korshunov, and I. I. Mazin, *Gap symmetry and structure of Fe-based superconductors*, Rep. Prog. Phys. **74**, 124508 (2011).
[7] M. Crespin, B. Y. P. Levitz, and L. Gatineau, *Reduced forms of* $LaNiO_3$ *perovskite*, J. Chem. Soc. **79**, 1181 (1983).
[8] M. A. Hayward, M. A. Green, M. J. Rosseinsky, and J. Sloan, *Sodium Hydride as a powerful reducing agent for*

topotactic oxide deintercalation: Synthesis and characterization of the nickel(I) oxide $LaNiO_2$, J. Am. Chem. Soc. **121**, 8843 (1999).

[9] M. Hayward and M. Rosseinsky, *Synthesis of the infinite layer* Ni(*I*) *phase* $NdNiO_{2+x}$ *by low temperature reduction of* $NdNiO_3$ *with sodium hydride*, Solid State Sci. **5**, 839 (2003).

[10] A. Ikeda, Y. Krockenberger, H. Irie, M. Naito, and H. Yamamoto, *Direct observation of infinite* NiO_2 *planes in* $LaNiO_2$ *films*, Appl. Phys. Express **9**, 061101 (2016).

[11] K. Lee, B. Y. Wang, M. Osada, B. H. Goodge, T. C. Wang, Y. Lee, S. Harvey, W. J. Kim, Y. Yu, C. Murthy, S. Raghu, L. F. Kourkoutis, and H. Y. Hwang, *Linear-in-temperature resistivity for optimally superconducting* $(Nd, Sr)NiO_2$, Nature (London) **619**, 288 (2023).

[12] P. Jiang, L. Si, Z. Liao, and Z. Zhong, *Electronic structure of rare-earth infinite-layer* $RNiO_2$ $(R = La, Nd)$, Phys. Rev. B **100**, 201106(R) (2019).

[13] A. S. Botana and M. R. Norman, *Similarities and differences between* $LaNiO_2$ *and* $CaCuO_2$ *and implications for superconductivity*, Phys. Rev. X **10**, 011024 (2020).

[14] M. Kitatani, L. Si, O. Janson, R. Arita, Z. Zhong, and K. Held, *Nickelate superconductors—A renaissance of the one-band Hubbard model*, npj Quantum Mater. **5**, 59 (2020).

[15] J. Karp, A. S. Botana, M. R. Norman, H. Park, M. Zingl, and A. Millis, *Many-body electronic structure of* $NdNiO_2$ *and* $CaCuO_2$, Phys. Rev. X **10**, 021061 (2020).

[16] H. Sakakibara, H. Usui, K. Suzuki, T. Kotani, H. Aoki, and K. Kuroki, *Model construction and a possibility of cupratelike pairing in a new* d^9 *nickelate superconductor* $(Nd, Sr)NiO_2$, Phys. Rev. Lett. **125**, 077003 (2020).

[17] S. Di Cataldo, P. Worm, J. M. Tomczak, L. Si, and K. Held, *Unconventional superconductivity without doping in infinite-layer nickelates under pressure*, Nat. Commun. **15**, 3952 (2024).

[18] H. Lu, M. Rossi, A. Nag, M. Osada, D. F. Li, K. Lee, B. Y. Wang, M. Garcia-Fernandez, S. Agrestini, Z. X. Shen, E. M. Been, B. Moritz, T. P. Devereaux, J. Zaanen, H. Y. Hwang, K.-J. Zhou, and W. S. Lee, *Magnetic excitations in infinite-layer nickelates*, Science **373**, 213 (2021).

[19] Y. Cui, C. Li, Q. Li, X. Zhu, Z. Hu, Y. F. Yang, J. Zhang, R. Yu, H. H. Wen, and W. Yu, *NMR evidence of antiferromagnetic spin fluctuations in* $Nd_{0.85}Sr_{0.15}NiO_2$, Chin. Phys. Lett. **38**, 067401 (2021).

[20] J. Fowlie, M. Hadjimichael, M. M. Martins, D. Li, M. Osada, B. Y. Wang, K. Lee, Y. Lee, Z. Salman, T. Prokscha, J.-M. Triscone, H. Y. Hwang, and A. Suter, *Intrinsic magnetism in superconducting infinite-layer nickelates*, Nat. Phys. **18**, 1043 (2022).

[21] M. Rossi *et al.*, *Universal orbital and magnetic structures in infinite-layer nickelates*, Phys. Rev. B **109**, 024512 (2024).

[22] F. Lechermann, *Late transition metal oxides with infinite-layer structure: Nickelates versus cuprates*, Phys. Rev. B **101**, 081110(R) (2020).

[23] M. Hepting *et al.*, *Electronic structure of the parent compound of superconducting infinite-layer nickelates*, Nat. Mater. **19**, 381 (2020).

[24] K.-W. Lee and W. E. Pickett, *Infinite-layer* $LaNiO_2$*:* Ni^{1+} *is not* Cu^{2+}, Phys. Rev. B **70**, 165109 (2004).

[25] M. Jiang, M. Berciu, and G. A. Sawatzky, *Critical nature of the* Ni *spin state in doped* $NdNiO_2$, Phys. Rev. Lett. **124**, 207004 (2020).

[26] M. Jiang, M. Berciu, and G. A. Sawatzky, *Stabilization of singlet hole-doped state in infinite-layer nickelate superconductors*, Phys. Rev. B **106**, 115150 (2022).

[27] D. Kaneko, K. Yamagishi, A. Tsukada, T. Manabe, and M. Naito, *Synthesis of infinite-layer* $LaNiO_2$ *films by metal organic decomposition*, Physica (Amsterdam) **469C**, 936 (2009).

[28] M. Kawai, S. Inoue, M. Mizumaki, N. Kawamura, N. Ichikawa, and Y. Shimakawa, *Reversible changes of epitaxial thin films from perovskite* $LaNiO_3$ *to infinite-layer structure* $LaNiO_2$, Appl. Phys. Lett. **94**, 082102 (2009).

[29] M. Osada, B. Y. Wang, B. H. Goodge, S. P. Harvey, K. Lee, D. Li, L. F. Kourkoutis, and H. Y. Hwang, *Nickelate superconductivity without rare earth magnetism:* $(La, Sr)NiO_2$, Adv. Mater. **33**, 2104083 (2021).

[30] K. Lee, B. H. Goodge, D. Li, M. Osada, B. Y. Wang, Y. Cui, L. F. Kourkoutis, and H. Y. Hwang, *Aspects of the synthesis of thin film superconducting infinite-layer nickelates*, APL Mater. **8**, 041107 (2020).

[31] G. Krieger, L. Martinelli, S. Zeng, L. E. Chow, K. Kummer, R. Arpaia, M. Moretti Sala, N. B. Brookes, A. Ariando, N. Viart, M. Salluzzo, G. Ghiringhelli, and D. Preziosi, *Charge and spin order dichotomy in* $NdNiO_2$ *driven by the capping layer*, Phys. Rev. Lett. **129**, 027002 (2022).

[32] G. Krieger, A. Raji, L. Schlur, G. Versini, C. Bouillet, M. Lenertz, J. Robert, A. Gloter, N. Viart, and D. Preziosi, *Synthesis of infinite-layer nickelates and influence of the capping-layer on magnetotransport*, J. Phys. D **56**, 024003 (2023).

[33] A. Ikeda, T. Manabe, and M. Naito, *Comparison of reduction agents in the synthesis of infinite-layer* $LaNiO_2$ *films*, Physica (Amsterdam) **506C**, 83 (2014).

[34] A. Ikeda, T. Manabe, and M. Naito, *Improved conductivity of infinite-layer* $LaNiO_2$ *thin films by metal organic decomposition*, Physica (Amsterdam) **495C**, 134 (2013).

[35] M. Osada, B. Y. Wang, B. H. Goodge, K. Lee, H. Yoon, K. Sakuma, D. Li, M. Miura, L. F. Kourkoutis, and H. Y. Hwang, *A superconducting praseodymium nickelate with infinite layer structure*, Nano Lett. **20**, 5735 (2020).

[36] S. Zeng, C. Li, L. E. Chow, Y. Cao, Z. Zhang, C. S. Tang, X. Yin, Z. S. Lim, J. Hu, P. Yang, and A. Ariando, *Superconductivity in infinite-layer nickelate* $La_{1-x}Ca_xNiO_2$ *thin films*, Sci. Adv. **8**, eabl9927 (2022).

[37] W. Wei, K. Shin, H. Hong, Y. Shin, A. S. Thind, Y. Yang, R. F. Klie, F. J. Walker, and C. H. Ahn, *Solid state reduction of nickelate thin films*, Phys. Rev. Mater. **7**, 013802 (2023).

[38] C. T. Parzyck, V. Anil, Y. Wu, B. H. Goodge, M. Roddy, L. F. Kourkoutis, D. G. Schlom, and K. M. Shen, *Synthesis of thin film infinite-layer nickelates by atomic hydrogen reduction: Clarifying the role of the capping layer*, APL Mater. **12**, 031132 (2024).

[39] B.-X. Wang, H. Zheng, E. Krivyakina, O. Chmaissem, P. P. Lopes, J. W. Lynn, L. C. Gallington, Y. Ren, S. Rosenkranz, J. F. Mitchell, and D. Phelan, *Synthesis and characterization of bulk* $Nd_{1-x}Sr_xNiO_2$ *and* $Nd_{1-x}Sr_xNiO_3$, Phys. Rev. Mater. **4**, 084409 (2020).

[40] P. Puphal, B. Wehinger, J. Nuss, K. Küster, U. Starke, G. Garbarino, B. Keimer, M. Isobe, and M. Hepting, *Synthesis and physical properties of* $LaNiO_2$ *crystals*, Phys. Rev. Mater. **7**, 014804 (2023).

[41] See Supplemental Material at http://link.aps.org/supplemental/10.1103/PhysRevX.15.021048, which includes Refs. [42–49], for further details concerning the resistivity, pulsed *I-V*, and Hall effect measurements as well as additional data from lab-based x-ray diffraction measurements, x-ray absorbtion spectroscopy measurements, and further STEM and DFT analysis of the effects of residual oxygen.

[42] B. Y. Wang, T. C. Wang, Y.-T. Hsu, M. Osada, K. Lee, C. Jia, C. Duffy, D. Li, J. Fowlie, M. R. Beasley, T. P. Devereaux, I. R. Fisher, N. E. Hussey, and H. Y. Hwang, *Effects of rare-earth magnetism on the superconducting upper critical field in infinite-layer nickelates*, Sci. Adv. **9**, eadf6655 (2023).

[43] L. Bhatt, C. T. Parzyck, N. Schnitzer, D. G. Schlom, K. M. Shen, B. H. Goodge, D. A. Muller, and L. F. Kourkoutis, *Resolving chemically driven charge ordering in infinite layer nickelates with multislice electron ptychography and 4D-STEM*, Microsc. Microanal. **30**, ozae044.743 (2024).

[44] A. Raji, G. Krieger, N. Viart, D. Preziosi, J. P. Rueff, and A. Gloter, *Charge distribution across capped and uncapped infinite-layer neodymium nickelate thin films*, Small **19**, 2304872 (2023).

[45] Y. Tokura, H. Takagi, and S. Uchida, *A superconducting copper oxide compound with electrons as the charge carriers*, Nature (London) **337**, 345 (1989).

[46] M. Kotiuga, Z. Zhang, J. Li, F. Rodolakis, H. Zhou, R. Sutarto, F. He, Q. Wang, Y. Sun, Y. Wang, N. A. Aghamiri, S. B. Hancock, L. P. Rokhinson, D. P. Landau, Y. Abate, J. W. Freeland, R. Comin, S. Ramanathan, and K. M. Rabe, *Carrier localization in perovskite nickelates from oxygen vacancies*, Proc. Natl. Acad. Sci. U.S.A. **116**, 21992 (2019).

[47] P. Giannozzi *et al.*, *QUANTUM ESPRESSO: A modular and open-source software project for quantum simulations of materials*, J. Phys. Condens. Matter **21**, 395502 (2009).

[48] P. Giannozzi *et al.*, *Advanced capabilities for materials modelling with QUANTUM ESPRESSO*, J. Phys. Condens. Matter **29**, 465901 (2017).

[49] G. Prandini, A. Marrazzo, I. E. Castelli, N. Mounet, and N. Marzari, *Precision and efficiency in solid-state pseudopotential calculations*, npj Comput. Mater. **4**, 72 (2018).

[50] D. Li, B. Y. Wang, K. Lee, S. P. Harvey, M. Osada, B. H. Goodge, L. F. Kourkoutis, and H. Y. Hwang, *Superconducting dome in* $Nd_{1-x}Sr_xNiO_2$ *infinite layer films*, Phys. Rev. Lett. **125**, 027001 (2020).

[51] C. C. Tam, J. Choi, X. Ding, S. Agrestini, A. Nag, M. Wu, B. Huang, H. Luo, P. Gao, M. García-Fernández, L. Qiao, and K.-J. Zhou, *Charge density waves in infinite-layer* $NdNiO_2$ *nickelates*, Nat. Mater. **21**, 1116 (2022).

[52] B. Cheng, D. Cheng, K. Lee, L. Luo, Z. Chen, Y. Lee, B. Y. Wang, M. Mootz, I. E. Perakis, Z.-X. Shen, H. Y. Hwang, and J. Wang, *Evidence for d-wave superconductivity of infinite-layer nickelates from low-energy electrodynamics*, Nat. Mater. **23**, 775 (2024).

[53] S. P. Harvey, B. Y. Wang, J. Fowlie, M. Osada, K. Lee, Y. Lee, D. Li, and H. Y. Hwang, *Evidence for nodal superconductivity in infinite-layer nickelates*, arXiv:2201.12971.

[54] A. J. Millis, S. Sachdev, and C. M. Varma, *Inelastic scattering and pair breaking in anisotropic and isotropic superconductors*, Phys. Rev. B **37**, 4975 (1988).

[55] R. J. Radtke, K. Levin, H.-B. Schüttler, and M. R. Norman, *Predictions for impurity-induced* T_c *suppression in the high-temperature superconductors*, Phys. Rev. B **48**, 653 (1993).

[56] Y. Lee, X. Wei, Y. Yu, L. Bhatt, K. Lee, B. H. Goodge, S. P. Harvey, B. Y. Wang, D. A. Muller, L. F. Kourkoutis, W.-S. Lee, S. Raghu, and H. Y. Hwang, *Synthesis of superconducting freestanding infinite-layer nickelate heterostructures on the millimetre scale*, Nat. Synth. (2025). 10.1038/s44160-024-00714-2

[57] Q. Gao, S. Fan, Q. Wang, J. Li, X. Ren, I. Biało, A. Drewanowski, P. Rothenbühler, J. Choi, R. Sutarto, Y. Wang, T. Xiang, J. Hu, K.-J. Zhou, V. Bisogni, R. Comin, J. Chang, J. Pelliciari, X. J. Zhou, and Z. Zhu, *Magnetic excitations in strained infinite-layer nickelate* $PrNiO_2$ *films*, Nat. Commun. **15**, 5576 (2024).

[58] F. M. Smits, *Measurement of sheet resistivities with the four-point probe*, Bell Syst. Tech. J. **37**, 711 (1958).

[59] W. Wei, D. Vu, Z. Zhang, F. J. Walker, and C. H. Ahn, *Superconducting* $Nd_{1-x}Eu_xNiO_2$ *thin films using in situ synthesis*, Sci. Adv. **9**, eadh3327 (2023).

[60] S.-W. Cheong, H. Hwang, B. Batlogg, A. Cooper, and P. Canfield, *Electron-hole doping of the metal-insulator transition compound* $RENiO_3$, Physica (Amsterdam) **194B–196B**, 1087 (1994).

[61] J. A. Alonso, M. J. Martínez-Lope, and M. A. Hidalgo, *Hole and electron doping of* $RNiO_3$ $(R = La, Nd)$, J. Solid State Chem. **116**, 146 (1995).

[62] H. Yang, Z. Wen, Y. Cui, Y. Chen, and Y. Zhao, *The preparation, structure, and metal-insulator transition in bulk* $Nd_{1-x}Ca_xNiO_3$ *(*$x = 0$–0.3*)*, J. Supercond. Novel Magn. **34**, 2339 (2021).

[63] R. K. Patel, K. Patra, S. K. Ojha, S. Kumar, S. Sarkar, A. Saha, N. Bhattacharya, J. W. Freeland, J. W. Kim, P. J. Ryan, P. Mahadevan, and S. Middey, *Hole doping in a negative charge transfer insulator*, Commun. Phys. **5**, 216 (2022).

[64] C. M. Brooks, L. F. Kourkoutis, T. Heeg, J. Schubert, D. A. Muller, and D. G. Schlom, *Growth of homoepitaxial* $SrTiO_3$ *thin films by molecular-beam epitaxy*, Appl. Phys. Lett. **94**, 3 (2009).

[65] C. M. Brooks, R. B. Wilson, A. Schäfer, J. A. Mundy, M. E. Holtz, D. A. Muller, J. Schubert, D. G. Cahill, and D. G. Schlom, *Tuning thermal conductivity in homoepitaxial* $SrTiO_3$ *films via defects*, Appl. Phys. Lett. **107**, 051902 (2015).

[66] C. T. Parzyck, N. K. Gupta, Y. Wu, V. Anil, L. Bhatt, M. Bouliane, R. Gong, B. Z. Gregory, A. Luo, R. Sutarto, F. He, Y.-D. Chuang, T. Zhou, G. Herranz, L. F. Kourkoutis, A. Singer, D. G. Schlom, D. G. Hawthorn, and K. M. Shen, *Absence of* $3a_0$ *charge density wave order in the infinite-layer nickelate* $NdNiO_2$, Nat. Mater. **23**, 486 (2024).

[67] M. Rossi, H. Lu, A. Nag, D. Li, M. Osada, K. Lee, B. Y. Wang, S. Agrestini, M. Garcia-Fernandez, J. J. Kas, Y.-D. Chuang, Z. X. Shen, H. Y. Hwang, B. Moritz, K.-J. Zhou, T. P. Devereaux, and W. S. Lee, *Orbital and spin character of doped carriers in infinite-layer nickelates*, Phys. Rev. B **104**, L220505 (2021).

[68] G. Krieger, H. Sahib, F. Rosa, M. Rath, Y. Chen, A. Raji, P. V. B. Pinho, C. Lefevre, G. Ghiringhelli, A. Gloter, N. Viart, M. Salluzzo, and D. Preziosi, *Signatures of canted antiferromagnetism in infinite-layer nickelates studied by x-ray magnetic dichroism*, Phys. Rev. B **110**, 195110 (2024).

[69] S. Zeng, C. S. Tang, X. Yin, C. Li, M. Li, Z. Huang, J. Hu, W. Liu, G. J. Omar, H. Jani, Z. S. Lim, K. Han, D. Wan, P. Yang, S. J. Pennycook, A. T. S. Wee, and A. Ariando, *Phase diagram and superconducting dome of infinite-layer* $Nd_{1-x}Sr_xNiO_2$ *thin films*, Phys. Rev. Lett. **125**, 147003 (2020).

[70] M. Osada, B. Y. Wang, K. Lee, D. Li, and H. Y. Hwang, *Phase diagram of infinite layer praseodymium nickelate* $Pr_{1-x}Sr_xNiO_2$ *thin films*, Phys. Rev. Mater. **4**, 121801(R) (2020).

[71] Y. Ando, A. N. Lavrov, S. Komiya, K. Segawa, and X. F. Sun, *Mobility of the doped holes and the antiferromagnetic correlations in underdoped high-*T_c *cuprates*, Phys. Rev. Lett. **87**, 017001 (2001).

[72] Y. Ando, S. Komiya, K. Segawa, S. Ono, and Y. Kurita, *Electronic phase diagram of high-*T_c *cuprate superconductors from a mapping of the in-plane resistivity curvature*, Phys. Rev. Lett. **93**, 267001 (2004).

[73] H. Sahib, A. Raji, F. Rosa, G. Merzoni, G. Ghiringhelli, M. Salluzzo, A. Gloter, N. Viart, and D. Preziosi, *Superconductivity in* $PrNiO_2$ *infinite layer nickelates*, Adv. Mater. **37**, 2416187 (2025).

[74] P. Richard, M. Neupane, Y.-M. Xu, P. Fournier, S. Li, P. Dai, Z. Wang, and H. Ding, *Competition between antiferromagnetism and superconductivity in the electron-doped cuprates triggered by oxygen reduction*, Phys. Rev. Lett. **99**, 157002 (2007).

[75] D. Song, S. R. Park, C. Kim, Y. Kim, C. Leem, S. Choi, W. Jung, Y. Koh, G. Han, Y. Yoshida, H. Eisaki, D. H. Lu, Z.-X. Shen, and C. Kim, *Oxygen-content-dependent electronic structures of electron-doped cuprates*, Phys. Rev. B **86**, 144520 (2012).

[76] N. Doiron-Leyraud, C. Proust, D. LeBoeuf, J. Levallois, J. Bonnemaison, R. Liang, D. Bonn, W. Hardy, and L. Taillefer, *Quantum oscillations and the Fermi surface in an underdoped high-*T_c *superconductor*, Nature (London) **447**, 565 (2007).

[77] I. Miccoli, F. Edler, H. Pfnür, and C. Tegenkamp, *The 100th anniversary of the four-point probe technique: The role of probe geometries in isotropic and anisotropic systems*, J. Phys. Condens. Matter **27**, 223201 (2015).

[78] B. H. Savitzky, I. El Baggari, C. B. Clement, E. Waite, B. H. Goodge, D. J. Baek, J. P. Sheckelton, C. Pasco, H. Nair, N. J. Schreiber, J. Hoffman, A. S. Admasu, J. Kim, S.-W. Cheong, A. Bhattacharya, D. G. Schlom, T. M. McQueen, R. Hovden, and L. F. Kourkoutis, *Image registration of low signal-to-noise cryo-STEM data*, Ultramicroscopy **191**, 56 (2018).

[79] S. Eisebitt, T. Böske, J.-E. Rubensson, and W. Eberhardt, *Determination of absorption coefficients for concentrated samples by fluorescence detection*, Phys. Rev. B **47**, 14103 (1993).

[80] A. J. Achkar, T. Z. Regier, H. Wadati, Y.-J. Kim, H. Zhang, and D. G. Hawthorn, *Bulk sensitive x-ray absorption spectroscopy free of self-absorption effects*, Phys. Rev. B **83**, 081106(R) (2011).

[81] Z. Dong, M. Hadjimichael, B. Mundet, J. Choi, C. C. Tam, M. Garcia-Fernandez, S. Agrestini, C. Domínguez, R. Bhatta, Y. Yu, Y. Liang, Z. Wu, J.-M. Triscone, C. Jia, K.-J. Zhou, and D. Li, *Topochemical synthesis and electronic structure of high-crystallinity infinite-layer nickelates on an orthorhombic substrate*, Nano Lett. **25**, 1233 (2025).

[82] Data acquired and analyzed during the course of the study are available at 10.34863/8x6a-m870.